Journal of Fluorine Chemistry 144 (2012) 137–142

Contents lists available at SciVerse ScienceDirect

Journal of Fluorine Chemistry

journal homepage: www.elsevier.com/locate/fluor

The study of the system Na_3AlF_6–FeF_3

František Šimko [a,*], Ondrej Prítula [a], Aydar Rakhmatullin [b], Catherine Bessada [b]

[a] Institute of Inorganic Chemistry, Slovak Academy of Sciences, Dúbravská cesta 9, 845 36 Bratislava, Slovakia
[b] Conditions Extrêmes et Matériaux: Haute Température et Irradiation CNRS, 1D av. de la Recherche Scientifique, 450 71 Orléans, France

ARTICLE INFO

Article history:
Received 21 December 2011
Received in revised form 9 July 2012
Accepted 25 August 2012
Available online 31 August 2012

Keywords:
Cryolite
Impurity
Rietveld method
MAS NMR analysis

ABSTRACT

Different techniques are used to understand the Na_3AlF_6–FeF_3 system behavior. Rietveld's structure refinement analysis is successfully applied to determine the lattice parameters as well as relative phase abundance of individual phases in the system Na_3AlF_6–FeF_3. The results confirm the presence of $Na_3(Al_xFe_y)F_6$ and $Na_5(Al_xFe_y)_3F_{14}$ ($x + y = 1$) solid solutions, depending on the amount of FeF_3 in the system. The system with 25 mol% FeF_3 contains crystalline phases in weight ratio: $64.8 \pm 2.8\%$ of $Na_3(Al_xFe_y)F_6$ and $35.2 \pm 2.7\%$ of $Na_5(Al_xFe_y)_3F_{14}$, respectively. In the first mentioned solution, the molar ratio of Al/Fe is 92.8/7.2 and 77.4/22.6 in second one. Weight loss measurements suggest that some new volatile products are emitted from the melt. MAS NMR investigations of the condensate exclude the presence of iron containing fluorides in the condensed sample and confirm that $NaAlF_4$ is the only vapor species, generating in the melted system.

1. Introduction

Iron belongs to predominant impurities that negatively influence the commercial production of aluminum, the Hall–Héroult process. In this process, liquid aluminum is produced by electrolytic reduction of alumina (Al_2O_3) which is dissolved in an electrolyte mainly containing cryolite (Na_3AlF_6) [1]. Iron compounds dissolved in the electrolyte may have a negative influence on the current efficiency of the process and on the resulting metal quality. They can participate in reactions with components of the electrolyte and change the electrolyte's chemical composition [2–4]. Thus, the classification of the mechanism of redox reactions of iron compounds with electrolyte components is needed. The present study is focused on the reactions taking place between FeF_3, and Na_3AlF_6. The traditional view implies that iron(III) compounds, like Fe_2O_3 or FeF_3 react in the electrolyte forming $FeF_6{}^{3-}$ species [5–7]. Diep studied the solubility of Fe_2O_3 as a function NaF/AlF_3 molar ratio with and without additions of alumina. The obtained data were used to interpret the ionic structure of iron compounds. The presence of a series considered iron-containing compounds that can be written in the general form as $Na_xFe_yF_z$ and $Na_xAl_qFe_yO_wF_z$ was suggested. Up to now, the system Na_3AlF_6–FeF_3 was examined only by Johansen [8]. There are indications that a eutectic is present at approximately 60 mol% FeF_3 at 694 °C. However, complementary analyses are necessary to pinpoint the curves defining phase boundaries [1].

The present paper studies the FeF_3 behavior in cryolite. The intention is to suggest possible processes that take place and to identify reaction products. However, it must be noted that it is impossible to investigate such a system in situ by usual techniques. The reasons are, e.g.: (i) XRD in melt lost its essential purpose (even some averaged structural information could be obtained, but this is out of the scope of this paper); (ii) NMR spectroscopy is useless when paramagnetic species are present. Thus, the following combination of techniques was used: (i) thermal analysis – as a basic method used to investigate molten salts; (ii) XRD and powder neutron diffraction of the quenched samples – in order to characterize reaction products; (iii) MAS NMR spectroscopy of condensed vapors in order to exclude the presence of iron and in order to confirm the suggested chemical reaction, where some of the products are volatile species. The presence of volatile products arises from TG measurements. The mosaic of particular results coming from different techniques can suggest some insight into the processes taking place in melts in spite of the fact that these indices are not direct proves that cannot be obtained (such a direct proofing would require, e.g. femtosecond spectroscopy).

2. Results and discussion

Thermal analysis with cryoscopy calculations was realized in order to study chemical reactions between components taking place in melts. Cryoscopy is a useful experimental method frequently applied for such investigations. For the lowering of

* Corresponding author. Tel.: +421 2 59410490; fax: +421 2 59410444.
E-mail address: uachsim@savba.sk (F. Šimko).

0022-1139/$ – see front matter © 2012 Elsevier B.V. All rights reserved.
http://dx.doi.org/10.1016/j.jfluchem.2012.08.007

the temperature of fusion of the solvent A, $\Delta_{fus}T(A)$, caused by the addition of the solute B the following equation holds

$$\Delta_{fus}T(A) = \frac{RT^2_{fus,A}}{\Delta_{fus}H_A} x_B k_{St} \quad (1)$$

where R is the gas constant, $T_{fus,A}$ and $\Delta_{fus}H_A$ is the temperature and enthalpy of fusion of the solvent A, respectively, x_B is the mole fraction of the solute B, and k_{St} is the semi-empirical correction factor introduced by Stortenbeker [13] representing the number of foreign particles, which introduces the solute B into the solvent A. Differentiating (Eq. (1)) according to x_A and setting for $x_A \to 1$ we get the relation for the tangent to the liquidus curve of the solvent A, k_0, at the temperature of fusion of the solvent A

$$\lim_{x_A \to 1} \frac{d(\Delta_{fus}T(A))}{dx_A} = \frac{RT^2_{fus,A}}{\Delta_{fus}H_A} k_{St} = k_0 \quad (2)$$

Knowing $T_{fus,A}$ and $\Delta_{fus}H_A$, from the tangent k_0 we can then calculate k_{St}, which enables one to elucidate the possible chemical reactions between components.

The experimentally determined values of temperature of primary crystallization of individual samples in the investigated system are given in Table 1.

The value of the Stortenbeker's correction factor was calculated from the tangent of the experimental liquidus curve of cryolite at the melting point of pure cryolite according to (Eq. (2)). For the enthalpy of fusion of cryolite the calorimetrically determined value was used [14]. The dependence of temperature of primary crystallization (T_{pc}) on $x_{Na_3AlF_6}$ was expressed in the form

$$\Delta T_{PC} = (190.4 \pm 1.7) - (190.4 \pm 1.8) \cdot x_{Na_3AlF_6} \quad (3)$$

The results of cryoscopic measurements for investigated system are shown in Fig. 2. For k_0 and k_{St} the values k_0 = 58.5 K and k_{St} = 0.46 were obtained, which indicate the introduction of approximately 0.5 new substances when 1 mol FeF_3 is dissolved in an infinite amount of cryolite (excluding the dissociation products of pure cryolite) [15]. This means that dissolving FeF_3 in cryolite half new particle is formed.

One can suggest the formation of a solid solution because the substitution of Fe^{3+} by Al^{3+} is known not to cause drastic crystallographic changes [16] and also because of similar crystallographic structure of Na_3FeF_6 and Na_3AlF_6. Both compounds posses monoclinic structure with similar space group (*P*1 21 1 for Na_3FeF_6, *P*1 21/n1 for Na_3AlF_6) [10,17] and dimensions of ionic radii of cations placed in the center of {FeF_6} and {AlF_6} octahedra (0.55 Å for Fe^{3+}, 0.54 Å for Al^{3+}) [18]. Therefore, iron has been shown to partially substitute aluminum in the cryolite structure and the substitution mechanism in the reaction process can be described as follows:

$$(3 + 2x)\ Na_3AlF_6(l) + (2 + 2y)\ FeF_3(l) = 2Na_3(Al_xFe_y)F_6(l) + 3\ NaAlF_4(g) \quad (4)$$

where $x + y = 1$.

The weight losses of investigated mixtures measured 1 h at 10–20 °C up to temperatures of its primary crystallization are summarized in Table 2.

The weight-loss of pure cryolite at 1020 °C was found to be 9.67%. It is well known that cryolite undergoes substantial thermal dissociation at melting under the formation of volatile $NaAlF_4$ and solid NaF, which remains in the bulk [19]. But in other samples 1 h weight-looses of melts further sharply increase with an increasing content of FeF_3 in comparison to pure cryolite. This effect can be caused by direct reaction of FeF_3 with cryolite in the melts. The result of such a process is that some volatile products are generated. This observation confirms the presence of volatile decomposition products originating from reactions in the system.

In order to confirm the above-mentioned suggestions, the capture of eventual gaseous reaction product(s) was realized by means of the developed apparatus (Fig. 1). According to realization of procedure described above the condensate product was obtained. It was placed in a Pt gatherer in the temperature region 700–800 °C (Fig. 1). The sum of weights of residue sample in Pt crucible and condensate product has shown that other volatile products cannot accrue (Fig. 2).

In the next steps, the condensate was homogenized and analyzed by solid state multinuclear (^{27}Al, ^{23}Na and ^{19}F) magnetic resonance spectroscopy with respect to higher sensitivity of this method compared to classical analytical methods (as for example X-ray diffraction analysis). The room temperature ^{27}Al MAS spectrum shows a peak about 1 kHz wide cantered at −13.5 ppm (Fig. 3, peak **A1**) (Table 3).

This signal belongs to a six-fold coordinated aluminum in {AlF_6} octahedral site of AlF_3 [20,21]. Moreover, the spectrum reveals two overlapping quadrupolar doublets. Booths represent two types of aluminum isotopes in structure of chiolite, $Na_5Al_3F_{14}$. The structure consists of alternating layers of corner-sharing {AlF_6} octahedral and distorted edge-sharing {NaF_6} octahedral. In all layers each fourth octahedron, having 2/m or 4/m symmetry, is replaced by a sodium atom. Two sodium atoms are coordinated by eight fluorine atoms and next eight sodium atoms by six fluorines. One {AlF_6} octahedron shares corners with four octahedra and next octahedron with two octahedra [11,20,22]. In the spectra the broader doublet (Fig. 3, peak **B1**) represents the Al site in {AlF_6} octahedron, which shares corners with two next-nearest-neighboring octahedral or with four next-nearest-neighboring octahedra (with δ_{iso}(**B1**) = −2.1 ppm and δ_{iso}(**A1**) = −3.2 ppm) [22] (Fig. 3, peak **C1**).

The ^{23}Na spectra contain only two broad overlapping quadrupolar doublets at δ_{iso} = −7.4 ppm and δ_{iso} = −20.7 ppm (Fig. 4, peaks **A2** and **B2**, respectively). They belong to two different Na sites in chiolite structure.

Table 1
Temperatures of primary crystallization in melts of the system Na_3AlF_6–FeF_3.

x (FeF_3)	t_{pc} (Na_3AlF_6) [°C]
0.000	1007.2
0.000	1007.1
0.010	1005.8
0.010	1006.2
0.020	1005.4
0.020	1005.9
0.030	1005.4
0.030	1005.2
0.050	1005.0
0.050	1004.3
0.075	1002.3
0.075	1002.6
0.100	1001.1
0.100	1000.9

Table 2
The weight-losses in the system Na_3AlF_6–x mol% FeF_3 (x = 0, 5, 25 and 40).

Weight [mg]	Sample	Δm (1020 °C), 1 h	
		[mg]	%
300	Empty run	−2.0	0.7
300	Pure Na_3AlF_6	−29.0	9.7
300	5 mol% FeF_3	−28.0	9.3
300	25 mol% FeF_3	−41.3	13.8
300	40 mol% FeF_3	−90.9	30.3

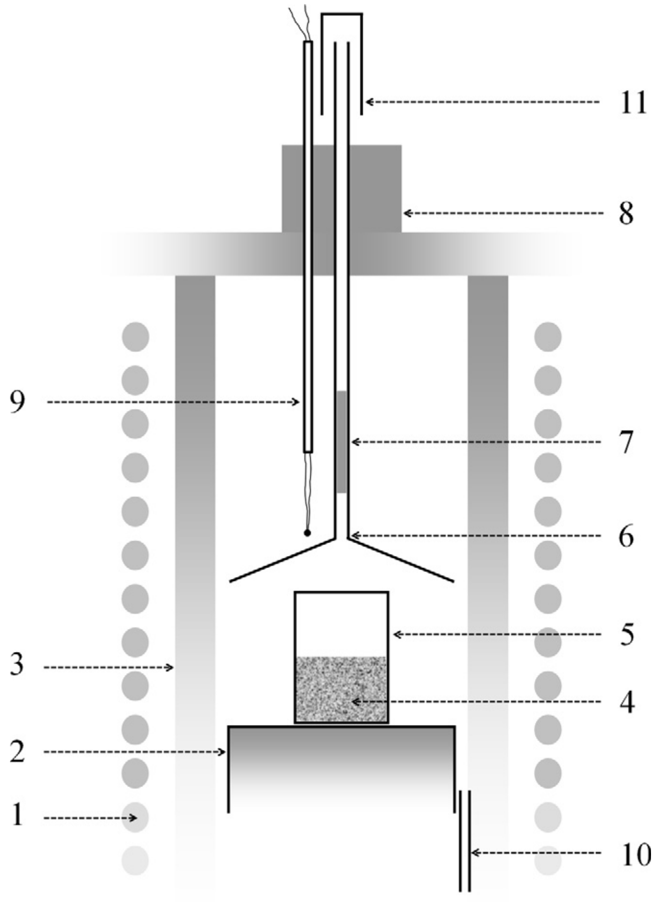

Fig. 1. The apparatus for the capturing of the volatile and condensed products; 1 – heating lines, 2 – Fe pad, 3 – Alsinth tube, 4 – sample, 5 – Pt crucible, 6 – Pt gatherer, 7 – condensed product, 8 – upper furnace cylinder, 9 – Pt/Pt10Rh thermocouple, 10 – argon input, and 11 – cylinder.

The ^{19}F spectrum shows four peaks. Resonances at −166.2, −182.0 and −191.0 ppm (Fig. 5 peaks **A3**, **D3** and **C3**, respectively) belong to three different F sites in chiolite structure [22,23]. There are three crystallographic fluorine sites in this compound, F(1), F(2) and F(3) with multiplicities of 4, 8 and 16, respectively. First fluorine site is coordinated by one Al(1) and four Na atoms (coordinated by six anions). The second fluorine site is bonded to

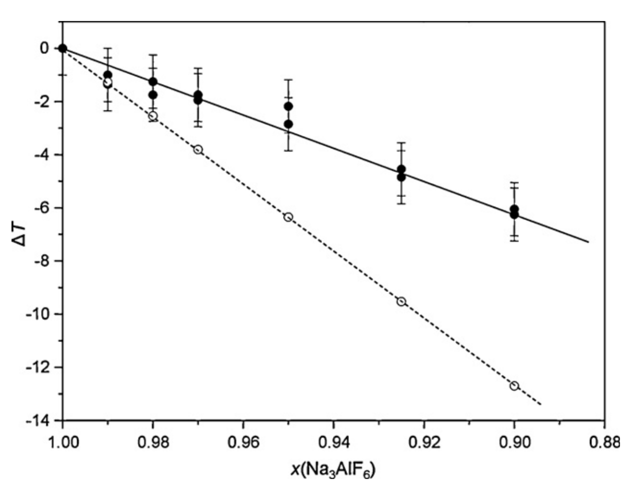

Fig. 2. Results of cryoscopic measurements in the system Na_3AlF_6–FeF_3; solid square – measured points, open square – calculated points for $k_{St} = 1$.

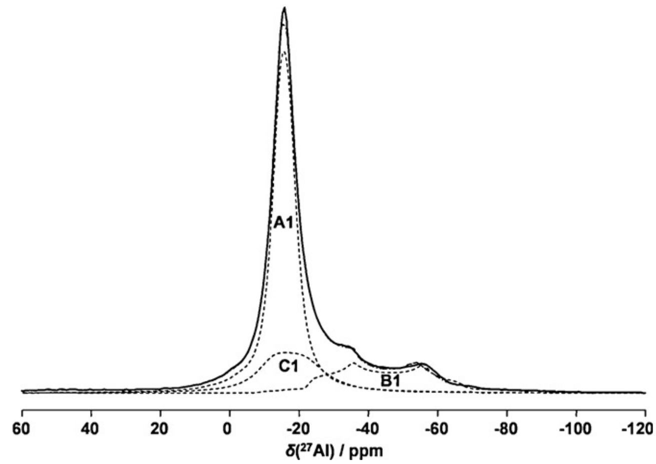

Fig. 3. Experimental (firm line) and simulated (full spectra – dash dot dash line, individual peaks – dotted lines) ^{27}Al MAS NMR spectrum of a condensed product of mixture Na_3AlF_6–40 mol% FeF_3.

Table 3
^{19}F, ^{27}Al and ^{23}Na isotropic chemical shifts, width (or broadening), quadrupolar coupling constants and anisotropy of the quadrupolar tensor from the fit of the MAS NMR spectral of the condensed sample in system Na_3AlF_6–40 mol% FeF_3.

Isotope	Sign of peak	δ_{iso} [ppm]	Width [kHz]	C_Q [MHz]	eta*Q*
^{19}F	A3	−166.2	1.80	–	–
	B3	−182.0	1.60	–	–
	C3	−191.0	1.40	–	–
	D3	−173.1	2.30	–	–
^{27}Al	A1	−13.5	0.50	0.4	0.03
	B1	−2.1	1.20	0.7	0.00
	C1	−3.2	0.22	1.0	0.34
^{23}Na	A2	−7.4	0.24	1.6	0.10
	B2	−20.7	0.17	0.8	0.01

two Al sites (Al(1) and Al(2)) and two more distant Na atoms (coordinated by six anions). The third fluorine is coordinated by one Al(2), one Na (coordinated by eight anion) and two Na atoms (coordinated by six anions). The resonance at $\delta_{iso} = -173$ ppm (Fig. 5, peak **B3**) is well-known signal assigned to F isotopes in regular $\{AlF_6\}$ octahedra of AlF_3.

The ^{19}F ^{23}Na and ^{27}Al MAS NMR spectra reveal two compounds in condensed product, namely $Na_5Al_3F_{14}$ and AlF_3. Moreover, experimental parameters (widths, chemical shifts, quadrupolar

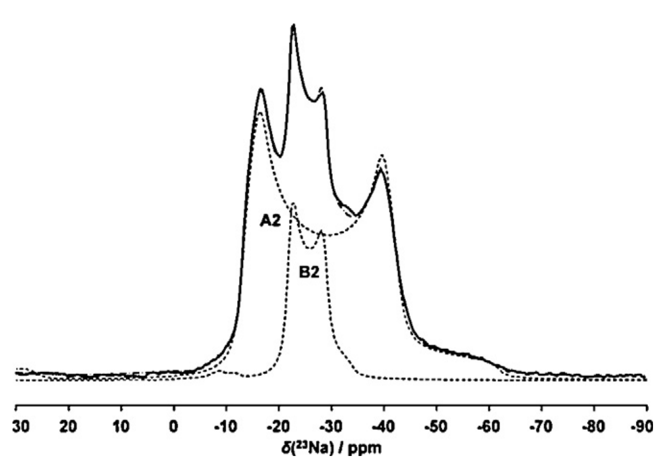

Fig. 4. Experimental (firm line) and simulated (full spectra – dash dot dash line, individual peaks – dotted lines) ^{23}Na MAS NMR spectrum of a condensed product of mixture Na_3AlF_6–40 mol% FeF_3.

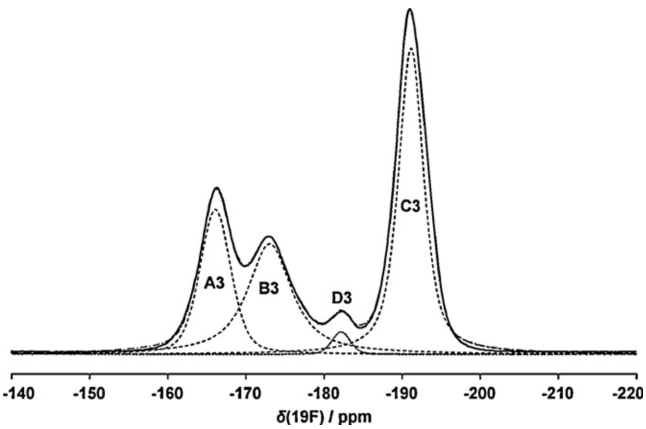

Fig. 5. Experimental (firm line) and simulated (full spectra – dash dot dash line, individual peaks – dotted lines) ^{19}F MAS NMR spectrum of a condensed product of mixture Na_3AlF_6–40 mol% FeF_3.

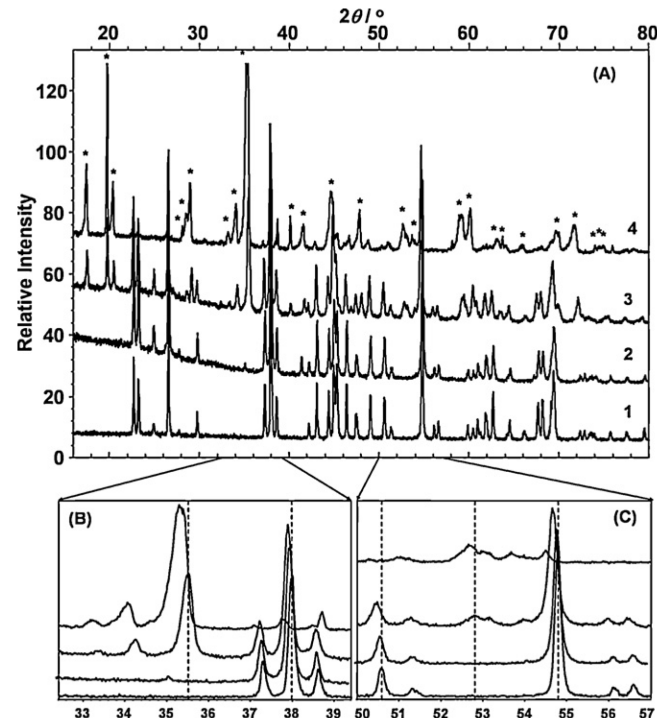

Fig. 6. Representative portions of the X-ray diffraction patterns of quickly quenched melts (A); (*) – $Na_5Al_3F_{14}$, (1) – Pure Na_3AlF_6, (2) – mixture with 10 mol% FeF_3, (3) – 25 mol% FeF_3, (4) – 50 mol% FeF_3. Five lines have been drawn in order to appreciate their shift to lower angles with increasing FeF_3 content (B and C).

parameters) of all signals are in agreement with published for pure compounds, which exclude the presence of paramagnetic Fe nuclei in this sample. The unpaired electrons of paramagnetic nuclei strongly shift the NMR resonance signal and enlarge the signal width. Therefore, the condensed product does not contain any paramagnetic Fe compounds.

The presence of $Na_5Al_3F_{14}$ and AlF_3 in the sample can be attributed to two sources. Firstly, cryolite undergoes substantial thermal dissociation at melting forming volatile $NaAlF_4$ and solid NaF, which remains in the bulk [19]. $NaAlF_4$ is a metastable compound and decomposes at 750 °C to $Na_5Al_3F_{14}$ and AlF_3 [24], according to Eq. (5).

$$5NaAlF_4(g) = 2AlF_3(s) + Na_5Al_3F_{14}(s) \quad (5)$$

The second source is the direct reaction of cryolite with FeF_3, which obviously resulted in the formation of $NaAlF_4$ (Eq. (4)).

Analyses of quenched samples are displayed in Fig. 6. It shows the XRD patterns of pure cryolite (line 1) and samples with various amounts of FeF_3 in mixture.

The X-ray diffraction patterns of pure cryolite and in a mixture with 10 mol% FeF_3 (line 2) are practically identical. The patterns of cryolite mixture with 25 mol% of FeF_3 (line 3) have shown new peaks, which fit with the XRD pattern. It corresponds to the known structure of chiolite, $Na_5Al_3F_{14}$ (PDFcard No. 72-548). From the XRD patterns of the solidified samples one can see that at lower FeF_3 concentrations the only crystallizing phase is cryolite. At higher concentrations of FeF_3, chiolite occurs as a new phase. Fig. 6B and C highlights the changes that take place in the XRD patterns. The positions of the peaks are changing due to each phase. This suggests that compositional variations are affecting the unit cell parameters and composition of cryolite and chiolite phases. Thus, one can conclude that changes in the XRD patterns are caused by the solid solution effect as was assumed above [16,18].

In order to calculate the dimensions of the unit cell of the first system member, the XRD and Neutron patterns of the sample with 25 mol% of FeF_3 have been analyzed using the Rietveld method (as described in Section 3.1). Reflections of the sample with 50 mol% FeF_3 could not be fitted for more diffuse X-ray pattern lines. Initial parameters for the refinement of the structure have been taken from those reported for pure Na_3AlF_6 and $Na_5Al_3F_{14}$ compounds, respectively (Table 4) [10,11].

Fig. 7 shows an example of graphical output of the Rietveld procedure illustrating the agreement between calculated and observed data. It can be observed that all reflections could be fitted on the basic of a monoclinic unit cell with space group *P*1 21/n1 and tetragonal unit cell with space group *P* 4/m n c, respectively. The lattice parameters for the pure compound, mixture and relevant volume unit cells are shown in Table 4. A very small shift of values for all tree cell parameters toward to compound parameters on the other side (Na_3FeF_6 a = 5.514(4), b = 5.734(3), and c = 7.973(6)) is shown [17]. One can suggest that the change in

Table 4
X-ray and neutron refined structural parameters Na_3AlF_6 [10], $Na_5Al_3F_{14}$ [11], and mixture Na_3AlF_6–25 mol% FeF_3.

Parameter	Na_3AlF_6 [10]	$Na_5Al_3F_{14}$ [11]	Sample: Na_3AlF_6–25 mol% FeF_3			
			Na_3AlF_6		$Na_5Al_3F_{14}$	
			X-ray	Neutron	X-ray	Neutron
a (Å)	5.4139(7)	7.0138(8)	5.4189(3)	5.4105(9)	7.1084(5)	7.096(1)
b (Å)	5.6012(5)	7.0138(8)	5.6096(3)	5.6046(9)	7.1084(5)	7.096(1)
c (Å)	7.7769(8)	10.402(2)	7.7927(5)	7.783(1)	10.422(1)	10.407(3)
α (°)	90	90	90	90	90	90
β (°)	90.183(3)	90	90.153(3)	90.142(2)	90	90
γ (°)	90	90	90	90	90	90
V (Å^3)	235.83	511.71	236.88(5)	235.99(3)	526.61(4)	524.02(4)

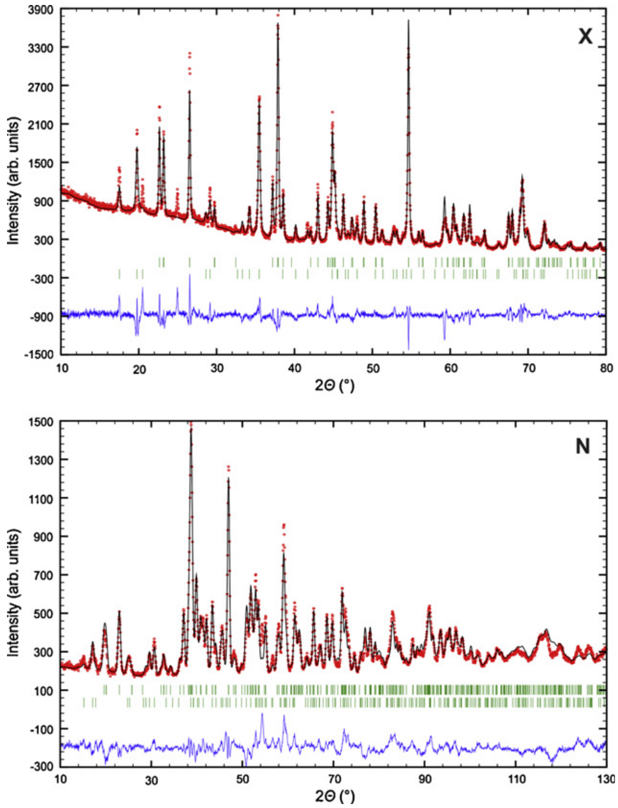

Fig. 7. Resulted Rietveld fits for the calculations with the X-ray (X) and the neutron (N) diffraction patterns. The peak at 24.5° 2θ in X-ray pattern belongs to the glue used to cover the sample a Mylard foil. Experimental patterns are shown as red dots, refined simulated patterns are shown as black line. The bottom solid lines show the difference between the calculated and observed intensities. (For interpretation of the references to color in this figure legend, the reader is referred to the web version of this article.)

unit cell and volume parameters from Na_3AlF_6 across intermediate mixtures to second corner specie is not linear but exponential. The same exponential increase in all unit cell parameters and volume with increasing FeF_3 content has previously been reported [16]. There is also an irregular variation of β with the composition of pure Na_3AlF_6 and Na_3FeF_6; 90.183(3)° and 90.42°, respectively [10,17]. It can be caused by the insensitivity of the angle β to changes in the interplanar spacing. Therefore, the value of β cannot be determined precisely [16]. It seems reasonable that replacing Al by Fe atom the c unit cell dimension leads to smaller modification because there is enough space along the c-axis for the Fe atoms to accommodate. However, the size of a and b parameters increases since the presence of a Fe atom causes expansion of the Fe–F octahedron in the a and b directions.

The same result is observed for chiolite. It belongs to the tetragonal space group $P\,4/m\,n\,c$ with two formula units per unit cell with dimensions a = 7.0138(8) Å, c = 10.402(2) Å [11]. The high-temperature form of $Na_5Fe_3F_{14}$ belongs to the tetragonal space group $P42\,21\,2$, also with two formula units per unit cell with dimensions a = 7.345(7) Å, c = 10.400(7) Å [25]. Although the space group of the Fe analog of chiolite is not its subgroup, single-crystal diffraction data confirm relationship and the possibility of solid solution formation. A very small shift of values of a and b axis and volume unit cell toward parameters of the $Na_5Fe_3F_{14}$ compound is also observed (volume cells 249.5 Å^3 for Na_3FeF_6 [16] and 561.07 Å^3 for $Na_5Fe_3F_{14}$ [25]). These results are in good agreement with the results of thermal analysis and cryoscopic calculations presented above.

The Rietveld analysis of the sample with 25 mol% of FeF_3 shows the composition of the crystalline components. This system contains 64.8 ± 2.8 wt% of $Na_3(Al_xFe_y)F_6$ phase and 35.2 ± 2.7 wt% of $Na_5(Al_xFe_y)_3F_{14}$ ($x + y = 1$) phase, respectively. The molar ratio of Al/Fe in "cryolite" solution is 92.8/7.2 and 77.4/22.6 in "chiolite" solution, respectively.

3. Conclusions

Solid solutions are evidenced and result from the substitution of Al^{3+} by Fe^{3+} in cryolite and chiolite structures. This observation has been concluded from cryoscopy analysis and XRD, Neutron/Rietveld results.

The formation of solid solution occurred along with the formation of volatile products in the investigated system. This observation was confirmed by standard weight loss tests. High sensitive ^{27}Al, ^{19}F and ^{23}Na MAS NMR analysis of condensed product defined that $NaAlF_4$ is the only volatile product in the system.

3.1. Experimental

The chemicals used in the studies were commercially available sodium fluoride (NaF, 99.5%, Merck, Germany), iron (III) fluoride (FeF_3, reagent grade, Aldrich, Germany) and self-made aluminum fluoride (AlF_3, min. 99.0%, sublimated, dried at 300 °C before use). All salts were handled in a glove box under dry inert nitrogen atmosphere (N_2, 99.99%, Messer) and measurements were performed under argon atmosphere (Ar, 99.996%, Messer). All experimental mixtures were prepared by mixing of synthetic cryolite (mixture of NaF and AlF_3 in mole ratio 3:1) with FeF_3.

The thermal effects data reported were obtained from cooling curves taken by ordinary thermal analysis. All homogenized mixtures used were placed in a Pt crucible and heated in a resistance furnace. Heating curves were recorded up to 50 °C up the complete melting of the mixture, with a heating rate of approximately 7 °C per minute. Then the cooling curves were recorded as well, however with the cooling rate that did not exceed 2 °C per minute. The temperatures of the mixtures were measured using a Pt/Pt10Rh thermocouple immersed directly into the melt. The thermocouple was calibrated to the melting point of pure sodium chloride (NaCl, 99.9%, Merck, Germany) and sodium fluoride with melting points 800.3 °C and 994.5 °C, respectively. The reproducibility of the measured temperatures was within ±1 °C.

Samples for quenching experiments were prepared by mixing synthetic cryolite and FeF_3. The compositions ranged from 0 to 50 mol% of FeF_3. The homogenized samples were placed in a Pt crucible and melted in a resistance furnace under the Argon atmosphere. Samples were heated up to 20 °C above their melting point. After equilibration, the melts were quenched in kerosene oil, placed in liquid nitrogen. Homogenized samples were analyzed by XRD and neutron diffraction methods at room temperature. X-ray diffraction patterns were collected within the interval of 10–80° in steps of 0.02° 2θ using Co Kα1 radiation. The samples were mounted on foils. To collect the X-ray patterns a transmission Stoe Stadi P diffractometer equipped with a linear PSD and a curved Ge(1 1 1) primary beam monochromator was used. Neutron diffraction data (N) were collected on the R2D2 diffractometer installed in the NFL, Studsvik, Sweden, using the wavelength of 1.5513 Å. This diffractometer is equipped with the vertically focusing Ge(5 1 1) monochromator with a fixed take-off angle of 90°. Samples were put to the vanadium containers. Calculations were done using FullProf2000 [9] program utilizing the monoclinic crystal structure of cryolite [10] and tetragonal structure of chiolite, $Na_5Al_3F_{14}$ [11]. In the calculations there, the selected profile and structure parameters for each model were refined, i.e. the scale factor + zero-point, halfwidth parameter *W* (in the case of the calculations for the neutron patterns also *U* and *V* halfwidth parameters), lattice parameters, atomic coordinates and the group temperature parameter Q (Å^2) for each type of atom. The strategy used in the refinements lied in the successive adding of the structural models to the refinements. In the first step the structural model of the phase with the highest expected weight content in the analyzed samples – cryolite – was introduced. When a refinement converged a chiolite phase was added to the calculations. The refinement was finished when all parameters of both phases were refined and when the calculation reached convergence.

Standard weight loss tests were carried out using a Q-1500D analyzer at inert argon atmosphere. In these experiments, the synthetic cryolite was mixed with various amount of FeF_3 (0, 5, 25, and 40 mol%). The samples were weighed before exposure by means of an analytical and a digital balance with a precision of 0.0001 g. Each mixture was set in Pt crucible and heated on temperature around 20 °C up the complete melting of the mixture, where the sample was kept 1 h. Specified heating rate did not exceed 7 °C per minute. The Pt/Pt10Rh thermocouple was used for the temperature measurements. The weight loss from time was recorded.

The special apparatus was designed for capture of eventual volatile species, condensed highly up to ambient temperature (Fig. 1). Pt gatherer was applied for prison of possible condensed product and was placed closely up to Pt crucible with sample. The homogenized mixture (20 g) with composition 60 mol% of cryolite and 40 mol% FeF_3 was placed in a Pt crucible and melted in a resistance furnace under Argon atmosphere, heated up to 20 °C above the temperature of primary crystallization and kept at this temperature for 2 h. The temperature of the mixture was measured using a Pt/Pt10Rh thermocouple placed up to Pt gatherer. Before the experiments, the thermal profile of furnace was made by reason of knowledge of temperature in place of sample replacement. Condensed products, obtained from gatherer, were homogenized on the powder and analyzed by MAS NMR methods.

All NMR experiments have been carried out with a Bruker AVANCE 400 (9.4 T) NMR spectrometer, operating at frequencies of 104.2 MHz for ^{27}Al, 105.8 MHz for ^{23}Na and 376.3 MHz for ^{19}F. The reported chemical shifts are referenced to 1 M solutions of NaCl, $Al(NO_3)_3$ for ^{23}Na, ^{27}Al, respectively, $CFCl_3$ for ^{19}F. Room temperature, magic angle spinning (MAS) NMR spectra have been acquired using high-speed MAS probe from Bruker, using 2.5 mm diameter rotors with a spinning rate of 34 kHz. In order to ensure good excitation conditions for both quadrupolar nuclei ^{27}Al, and ^{23}Na, very short pulses of 0.5 μs were used with recycle times of 500 ms. Around 1024 scans were acquired for ^{19}F experiments and up to 100 000 for ^{27}Al and ^{23}Na. All NMR spectra were modeled using the Dmfit program [12].

Acknowledgments

This work was supported by the EEC, Contract HPMC-CT-2000-00169 in the frame of the Marie Curie training site "high resolution solid/high temperature liquid Nuclear Magnetic Resonance in Materials sciences" (Orleans, France), and Slovak Grant Agency (VEGA-2/0179/10 and 2/0058/09). This publication is the result of the project implementation: Center for materials, layers and systems for applications and chemical processes under extreme conditions supported by the Research & Development Operational Program funded by the ERDF.

References

[1] J. Thonstad, P. Fellner, G.M. Haarberg, J. Híveš, H. Kvande, A. Sterten, Aluminium Electrolysis, Fundamentals of the Hall–Héroult Process, 3rd ed., Aluminium Verlag GmbH, Düsseldorf, 2001 .
[2] Å. Sterten, P.A. Solli, E. Skybakmoen, Journal of Applied Electrochemistry 28 (1998) 781–789.
[3] P.A. Solli, G.M. Haarberg, T. Eggen, E. Skybakmoen, A. Sterten, Light Metals (1994) 195–203.
[4] Å. Sterten, Light Metals (1991) 445–452.
[5] Q.B. Diep, Dr. -Ing. Thesis, Norwegian University of Science and Technology, Trondheim, 1998.
[6] F. Šimko, V. Daněk, Chemical Papers 55 (2001) 269–272.
[7] F. Šimko, I. Proks, V. Daněk, M. Boča, M. Chrenková, Zeitschrift fur Physikalische Chemie 218 (2004) 1213–1223.
[8] H.G. Johansen, Dr. -Ing. Thesis, Norwegian University of Science and Technology, Trondheim, 1975.
[9] J. Rodriguez-Carvajal, FullProf2000, 2000 http://www-llb.cea.fr/fullweb/fp2k.
[10] H.-X. Yang, S. Ghose, D.M. Hatch, Physics and Chemistry of Minerals 19 (1993) 528–544.
[11] C. Jacoboni, A. Leble, J.J. Rousseau, Journal of Solid State Chemistry 36 (1981) 297–304.
[12] D. Massiot, F. Fayon, M. Capron, I. King, S. Le Calvé, B. Alonso, J.-O. Durand, B. Bujoli, Z. Gan, G. Hoatson, Magnetic Resonance in Chemistry 40 (2002) 70–76.
[13] W. Stortenbeker, Zeitschrift für Physikalische Chemie 10 (1892) 183–186.
[14] Å. Sterten, I. Mæland, Acta Chemica Scandinavica 39 (1985) 241–247.
[15] I. Proks, V. Daněk, M. Chrenková, F. Šimko, Z. Pánek, Chemical Papers 56 (2002) 71–76.
[16] W.J. Croft, M. Kestigian, Materials Research Bulletin 3 (1968) 571–576.
[17] E.N. Matvienko, O.V. Jakubovich, M.A. Simonov, A.N. Ivashchenko, O.K. Mel'nikov, N.V. Belov, Doklady Akademii Nauk SSSR 257 (1981) 105–108 (Phase Transition 38 (1992) 127-220).
[18] D.R. Lide (Ed.), 82nd ed., Handbook of Chemistry and Physics, vol. 12–14, 2001–2002.
[19] M. Bruno, O. Herstad, J.L. Holm, Acta Chemica Scandinavica 52 (1998) 1399–1406.
[20] P.J. Dirken, J.B.H. Jansen, R.D. Schuiling, American Mineralogist 77 (1992) 718–724.
[21] J.F. Stebbins, I. Farnan, N. Dando, S.-Y. Tzeng, Journal of the American Ceramic Society 75 (1992) 3001–3006.
[22] D.R. Spearing, J.F. Stebbins, I. Farnan, Physics and Chemistry of Minerals 21 (1994) 373–386.
[23] V. Lacassagne, C. Bessada, P. Florian, S. Bouvet, B. Ollivier, J.-P. Coutures, D. Massiot, Journal of Physical Chemistry B 106 (2002) 1862–1868.
[24] O. Bjørseth, O. Herstad, J.L. Holm, Acta Chemica Scandinavica A40 (1986) 566–571.
[25] M. Vlasse, F. Menil, C. Moriliere, J.M. Dance, A. Tressaud, J. Portier, Journal of Solid State Chemistry 17 (1976) 291–298.